Neurobiology of Disease

Impaired Limbic Gamma Oscillatory Synchrony during Anxiety-Related Behavior in a Genetic Mouse Model of Bipolar Mania

Kafui Dzirasa,[1,4] DeAnna L. McGarity,[2] Anirban Bhattacharya,[6] Sunil Kumar,[1] Joseph S. Takahashi,[7] David Dunson,[6] Colleen A. McClung,[8] and Miguel A. L. Nicolelis[2,3,4,5,9]

[1]Department of Psychiatry and Behavioral Sciences, [2]Department of Neurobiology, [3]Department of Psychology and Neuroscience, [4]Center for Neuroengineering, and [5]Department of Biomedical Engineering, Duke University Medical Center, Durham, North Carolina 27710, [6]Department of Statistical Sciences, Duke University, Durham, North Carolina 27708, [7]Department of Neuroscience, Howard Hughes Medical Institute, [8]Department of Psychiatry, University of Texas Southwestern Medical Center, Dallas, Texas 75390-9111, and [9]Edmond and Lily Safra International Institute of Neuroscience of Natal, 59066-060 Natal, Brazil

Alterations in anxiety-related processing are observed across many neuropsychiatric disorders, including bipolar disorder. Though polymorphisms in a number of circadian genes confer risk for this disorder, little is known about how changes in circadian gene function disrupt brain circuits critical for anxiety-related processing. Here we characterize neurophysiological activity simultaneously across five limbic brain areas (nucleus accumbens, amygdala, prelimbic cortex, ventral hippocampus, and ventral tegmental area) as wild-type (WT) mice and mice with a mutation in the circadian gene, CLOCK (*Clock*-Δ19 mice) perform an elevated zero maze task. In WT mice, basal limbic gamma oscillatory synchrony observed before task performance predicted future anxiety-related behaviors. Additionally, dynamic changes in limbic gamma oscillatory synchrony were observed based on the position of WT mice in the zero maze. *Clock*-Δ19 mice, which displayed an increased propensity to enter the open section of the elevated maze, showed profound deficits in these anxiety-related circuit processes. Thus, our findings link the anxiety-related behavioral deficits observed in *Clock*-Δ19 mice with dysfunctional gamma oscillatory tuning across limbic circuits and suggest that alterations in limbic oscillatory circuit function induced by circadian gene polymorphisms may contribute to the behavioral manifestations seen in bipolar mania.

Introduction

Anxiety is a complex behavioral phenomenon resulting from dynamic interactions between an organism and its surrounding environment. Alterations in anxiety processing have been observed across many human neuropsychiatric disorders including generalized anxiety disorder, obsessive compulsive disorder, posttraumatic stress disorder, bipolar disorder, and depression (American Psychiatric Association, 2000). Given that the anxiety dysfunction in many of these disease states is associated with excessive or absent fear, considerable effort has been made to uncover the brain networks involved in central fear-related processing. Studies in humans have demonstrated that several limbic brain areas play a key role in modulating the expression, consolidation, and extinction of fear (Shin and Liberzon, 2010). For example, functional imaging studies have shown that amygdalar networks are activated during exposure to fearful stimuli (LaBar et al., 1998), whereas prefrontal cortical networks are activated during fear extinction (Kalisch et al., 2006). Moreover, evidence has suggested that alterations in cortical–striatal signaling may contribute to the behavioral manifestations seen in anxiety-related behavioral disturbances, such as obsessive compulsive disorder (Aouizerate et al., 2004; Greenberg et al., 2010). Notably, since the anxiety-related behavioral changes observed across neuropsychiatric disorders likely result from brain circuit changes that occur on the microscopic level, several studies have been conducted in rodents in an effort to identify neurophysiological circuits that contribute to fear processing (Seidenbecher et al., 2003; Gordon et al., 2005; Laviolette et al., 2005; Adhikari et al., 2010).

Anxiety has been classically modeled in rodents using behavioral tasks that quantify the effect of anxiogenic stimuli on the exploratory drive of individual animals. The elevated plus maze is one such task in which anxiety in modeled based on the tendency of an animal to explore the open sections of an elevated platform versus its tendency to explore the closed sections (Crawley, 1999) (see Fig. 1*a*). Since the aversive stimulus used in the task (i.e., elevated open arm) is based on an animal's intrinsic acute fear

Received Nov. 24, 2010; revised Feb. 7, 2011; accepted Feb. 27, 2011.

Author contributions: K.D., D.M., C.A.M., and M.A.N. designed research; K.D., D.M., and S.K. performed research; K.D., D.M., A.B., D.D., and C.A.M. analyzed data; K.D., A.B., S.K., J.S.T., D.D., C.A.M., and M.A.N. wrote the paper.

This work was supported by funding from UNCF/Merck, and National Institute of Mental Health (NIMH) Grant P50MH060451 to K.D.; National Institute on Drug Abuse, NIMH, The Blue Gator Foundation, The McKnight Foundation, and the National Alliance for Research on Schizophrenia and Depression to C.A.M.; and by National Institutes of Health Grant P50MH060451 and The Safra Foundation to M.A.L.N. We thank L. Oliveira, T. Jones, and G. Wood for miscellaneous support; H. Zhang for comments on this manuscript; S. Halkiotis for proofreading of this manuscript; and G. Lehew and H. W. Phillips for constructing the elevated zero maze used for neurophysiological recordings. A special thanks to Freeman Hrabowski, Robert and Jane Meyerhoff, and the Meyerhoff Scholarship Program.

Correspondence should be addressed to Dr. Kafui Dzirasa, Department of Psychiatry and Behavioral Sciences, Duke University Medical Center, 333 Bryan Research Building, Durham, NC 27710. E-mail: kafui.dzirasa@duke.edu.

DOI:10.1523/JNEUROSCI.6144-10.2011

 0270-6474/11/316449-08$15.00/0

response, task performance does not require pairing with a conditioned stimulus. Mice with an *N*-ethyl-*N*-nitrosurea-induced point mutation in the circadian gene *Clock* (*Clock*-Δ19 mice) (Vitaterna et al., 1994; King et al., 1997) display profound deficits in anxiety-related behaviors. For example, studies have demonstrated that *Clock*-Δ19 mice show an increased number of entries into the open arms of an elevated plus maze (Roybal et al., 2007). In addition, they spend more time in the center of an open field, have more entries into the light side of a dark/light box, and have a decreased latency to approach other innately aversive stimuli (i.e., bobcat urine) (Roybal et al., 2007). Because of these abnormalities, as well as others involving the mood and reward system (Dzirasa et al., 2010), *Clock*-Δ19 mice have been proposed as a genetic mouse model of bipolar mania (Roybal et al., 2007). Importantly, many of the behavioral abnormalities exhibited by *Clock*-Δ19 mice are ameliorated by treatment with lithium (an agent used to treat similar behavioral endophenotypes in human bipolar patients) (Roybal et al., 2007).

Materials and Methods

Animal care and use. *Clock*-Δ19 mice were created by *N*-ethyl-*N*-nitrosurea mutagenesis and produce a dominant-negative CLOCK protein as previously described (King et al., 1997). All animals used in this study were bred from heterozygous ($Clock^{\Delta 19/+}$) breeding pairs on a BALB/cJ and C57BL/6J mixed-strain background. Male *Clock*-Δ19 ($Clock^{\Delta 19}/Clock^{\Delta 19}$) and wild-type (WT; +/+) littermate controls, 20–30 weeks old, were used for all electrophysiological experiments presented in this study. Mice were housed on a 12 h light/dark cycle, three to five per cage, and maintained in a humidity- and temperature-controlled room with water available *ad libitum*. Eight *Clock*-Δ19 mice and 10 WT littermate controls were separated into individual cages and surgically implanted with recording electrodes. Experiments were initiated following a 2 week recovery and animals were exposed to the zero maze only once. Experiments were conducted for 10 min while animal were in their home cage and for 10 min as mice explored a zero plus maze during the first 6 h of the light cycle.

All studies were conducted with approved protocols from the Duke University Institutional Animal Care and Use Committee and were in accordance with the NIH Guidelines for the Care and Use of Laboratory Animals.

Zero maze task behavioral scoring. The zero maze was constructed from wood and the dimensions were as follows: the maze was elevated 31.25 inches from the ground, with an outer diameter of 19.5 inches, an inner diameter of 15.75 inches, and a wall height of 6 inches. Each mouse was placed in a closed section of the zero maze at the beginning of the task and was allowed to explore the maze for 10 min. All animals that fell off of the maze before the completion of the 10 min recording period (one WT and three *Clock*-Δ19 mice) were excluded from the study. A semiautomated technique was used to determine the speed and acceleration profiles of mice as they performed the zero-maze task. Overhead video recordings were digitized at 30 frames per second, and the location of the animals' headstage was manually scored every 0.5 s. The instantaneous speed and acceleration profiles of mice were then extrapolated from these data. Since this scoring approach erroneously located mice in the open segments of the maze during periods when mice were in the closed segment and peering out into the open segment (center of mass and all four paws in the closed segment, head stretched into the open segment), we used a more stringent method for identifying true open- and closed-segment intervals. The true position of mice on the zero maze was scored from video-recorded data for every 1 s interval of task performance. All data were scored by an observer that was blind to genotype. An animal's location was scored as 0 if all four paws of an animal's paws were completely within a closed segment of the zero maze for the entire 1 s interval, and an animal's location was scored as 1 if all four of the animals paws were in the open segment of the maze for the entire 1 s interval. Transition periods, or periods when an animal paused halfway between an open and closed segment, were scored as 0.5. Two anxiety-related behavioral indices were then calculated for each mouse: the open-segment time (the percentage of time a mouse spent in the open segment during the 10 min session), and the open-segment entries (the number of times that a mouse moved from the closed-segment into an open-segment of the maze during the 10 min session). Only open (1) and closed (0) periods were used for local field potentials (LFP) synchrony and LFP oscillatory power analysis performed at zero temporal offsets.

Table 1. Implantation coordinates for tungsten microwires

Area	AP (mm)	ML (mm)	DV (mm)
Nucleus accumbens	+1.25	+1.15	−3.9
Prelimbic cortex	+2.4	+0.25	−1.0
Amygdala	−1.6	−2.5	−4.75
Ventral hippocampus	−3.3	+2.75	−3.75
VTA	−3.2	+0.3	−4.25

All coordinates measured from bregma. AP, Anterior-posterior; ML, mediolateral; DV, dorsal-ventral.

Surgery. *Clock*-Δ19 mice and WT littermate controls were anesthetized with ketamine (100 mg/kg) and xylazine (10 mg/kg), placed in a stereotaxic device, and metal ground screws were secured to the cranium. A total of 32–48 tungsten microwires were arranged in array bundles (Dzirasa et al., 2011) and implanted as shown in Table 1. Implanted electrodes were anchored to ground screws using dental acrylic. All 10 WT and eight *Clock*-Δ19 animals were implanted in nucleus accumbens and two to four additional brain areas.

Neuronal and LFP data acquisition. Neuronal activity was sorted online and recorded using the Multi-Neuron Acquisition Processor system (Plexon). At the end of the recording, cells were sorted again using an offline sorting algorithm based on cluster analysis (Plexson) to confirm the quality of the recorded cells. Only clearly defined cell clusters were used for analysis. LFPs were preamplified (500×), filtered (0.5–400 Hz), and digitized at 500 Hz using a digital acquisition card (National Instruments) and the Multi-Neuron Acquisition Processor (Plexon). All electrophysiological recordings were referenced to two ground screws and recording segments demonstrating LFP saturation resulting from movement artifacts were excluded from analysis. LFPs were recorded from every implanted tungsten electrode. It is important to note that LFP recordings were associated with significant phase offsets that varied across frequencies (Nelson et al., 2008). These phase offsets were corrected using the FPAlign function (Plexon).

Determination of phase locking. LFPs were filtered using Butterworth bandpass filters designed to isolate LFP oscillations within the low-gamma (30–50 Hz) frequency range. High-amplitude low-gamma LFP segments (>2 SD of mean oscillatory amplitude) were also identified from the filtered LFP. The instantaneous phase of the filtered LFP was then determined using the Hilbert transform and phase locking was detected for both low-gamma traces and high-amplitude low-gamma segments using the Rayleigh test at $\alpha = 0.05$ (Siapas et al., 2005; Jacobs et al., 2007). Since phase-locking analysis is highly influenced by the number of spike events used for analysis, we fixed the total number of spike events used to quantify low-gamma phase locking to the number of spikes that occurred during high-amplitude low-gamma segments for each cell. This allowed for phase-locking comparisons between low-gamma segments and high-amplitude low-gamma segments. Cells that fired <50 times during the high-amplitude low-gamma segments were excluded from this study [five of 23 nucleus accumbens (NAC) cells in WT mice, three of 27 NAC cells in *Clock*-Δ19 mice].

Determination of LFP cross-structural synchrony. Half of the microwires implanted in each structure (two to four microwires) were randomly selected for LFP analysis. LFP cross-structural coherence was then calculated from LFP pairs using the Matlab (MathWorks) *mscohere* function at a 1 s sliding window with a 1 s step. The transform parameters were chosen to allow for a frequency resolution of 0.5 Hz. This process yielded up to 16 continuous cross-structural synchrony values and the overall cross-structural synchrony was given as the average of the four cross-structural LFP channel combinations that demonstrated the highest mean baseline synchrony for each cross-structural synchrony comparison. The LFP synchrony values used for analysis were then defined as the synchrony value for a particular second within each frequency band of interest normalized by the mean LFP synchrony observed within the

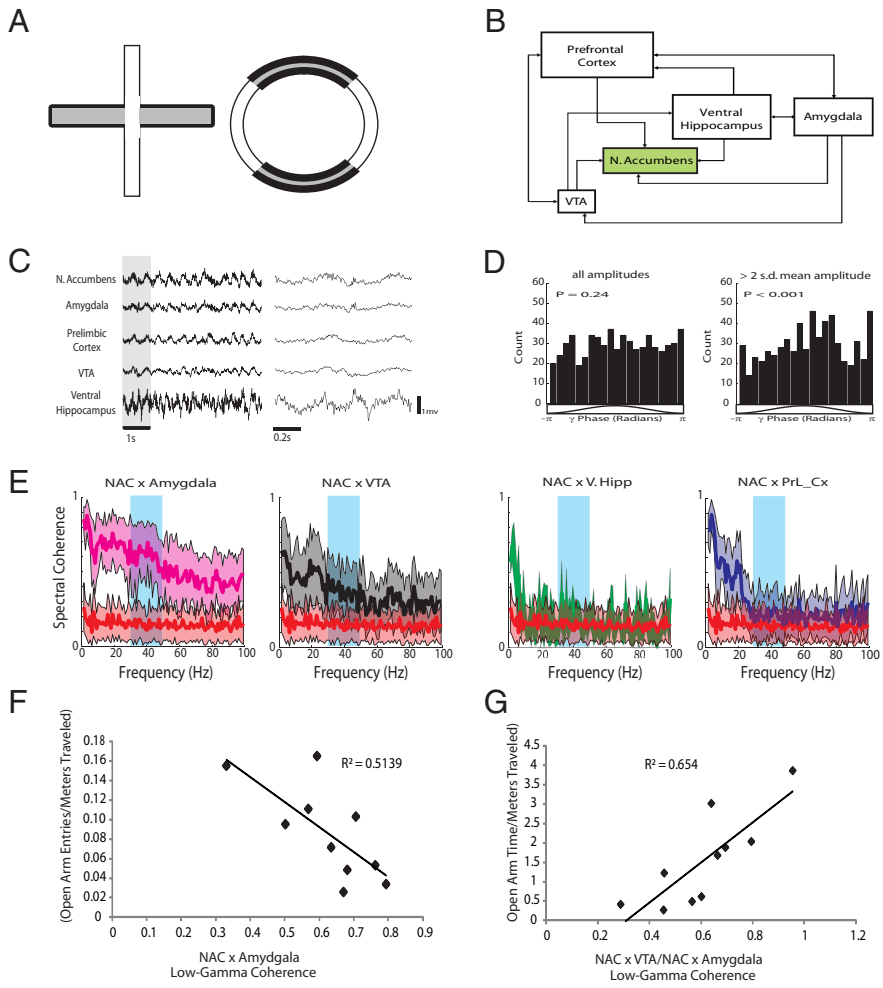

Figure 1. Limbic low-gamma synchrony predicts anxiety-related behaviors. ***A***, Diagram of a classic elevated plus maze and the zero maze used for this study. Shaded sections represent closed segments; unshaded sections represent open segments. ***B***, Diagram of limbic circuit involved in anxiety regulation. ***C***, Five second trace of LFPs recorded simultaneously from nucleus (N.) accumbens, VTA, prelimbic cortex, amygdala, and ventral hippocampus in awake behaving mouse. The first second of each LFP trace (gray shading) is shown at a higher time scale resolution to the right. ***D***, Phase distribution of NAC neuron. The neuron only displayed phase-locking to low-gamma oscillations during high low-gamma amplitude LFP segments (>2 SD of mean oscillatory amplitude) (right vs left). ***E***, Cross spectral synchrony between NAC and BA, VTA, ventral hippocampus (V. Hipp), and PrL_Cx in WT mice ($n = 824$, 709, 143, and 547 LFP pairs, respectively; mean ± SD, synchrony thresholds calculated using our bootstrapping method are shown in red). ***F***, ***G***, Home cage spectral coherence correlates with anxiety-related behaviors in WT mice. Regression lines are shown in black.

same frequency band observed during the baseline period. These normalization procedures were done to stabilize the variance in synchrony values observed across LFP channel combinations and animals.

Determination of LFP oscillatory power. Using Matlab, a sliding-window Fourier transform was applied to the LFP signal using a 1 s window with a 1 s step. The Fourier transform parameters were then chosen to allow for a frequency resolution of 0.5 Hz. The LFP oscillatory power values used for analysis were then assigned as the mean power within each frequency band of interest observed across the LFP channels used for synchrony analysis normalized by the mean LFP oscillatory power observed in the home cage.

Statistics. Longitudinal data are commonly encountered in many application areas. A longitudinal dataset essentially comprises of a response variable y_{it} and a $p \times 1$ vector of covariates x_{it} observed at times $t = 1, \ldots, n_i$ for subjects $i = 1, \ldots, N$. In such settings, one of the key aspects is to take into account the possible dependence among the repeated observations on a particular subject. If the response variable is continuous, one can potentially use the mixed effects model of Laird and Ware (1982). For binary or categorical response, it is difficult to specify a joint distribution for the repeated measurements y_{it}; $t = 1, \ldots, n_i$ directly. Zeger and Liang (1986) proposed a method of generalized estimating equations (GEE), which instead use a working generalized linear model for the marginal distribution of y_{it}. A working estimate of the regression coefficients is obtained under the assumption that the repeated measurements are independent, which is improved upon by accounting for within-subject dependence. Let y_{it} denote the position (1 = open, 0 = closed) of the i^{th} mouse at time t and x_{it} denote a vector of covariates consisting of the synchrony or neural oscillatory power corresponding to different brain regions and frequency ranges. The GEE was fitted using the GEEQBOX software in MATLAB. We assumed a first-order autoregressive working correlation structure. The p values for testing significance of the regression coefficients are reported. A Bonferroni correction was then applied to reported p values to determine statistical significance.

Results

Clock-Δ19 mice exhibit alterations in nucleus accumbens low-gamma (30–50 Hz) intranetwork synchrony (Dzirasa et al., 2010). Moreover, this frequency and brain area-specific neurophysiological deficit is ameliorated by chronic treatment with lithium (Dzirasa et al., 2010). Together, these findings raise the hypothesis that deficits in NAC low-gamma synchrony may contribute to the circuit-level impairments that mediate the mania-like behavioral manifestations resulting from disrupted *Clock* gene function. To directly test this hypothesis, we set out to determine whether nucleus accumbens low-gamma oscillatory activity contributes to the synchronization of vast mesolimbic networks underlying the normal manifestation of anxiety-related behaviors in healthy mice, and whether deficits in this neural oscillatory mode contribute to the circuit-level impairments that mediate anxiety-related behavioral dysfunction in *Clock*-Δ19 mice. Thus, we conducted neurophysiological recordings simultaneously across nucleus accumbens and four additional limbic brain areas that contribute afferent inputs to this brain area [prelimbic cortex (PrL_Cx), basolateral/basomedial amygdala (BA), ventral hippocampus (V. Hipp), and ventral tegmental area (VTA)] (Fig. 1*B*) (Swanson, 1982; Brog et al., 1993) as WT and *Clock*-Δ19 mice performed an elevated zero-maze task (a modified version of the elevated plus maze).

Mice implanted with microelectrodes recovered well and behaved normally, allowing us to simultaneously record LFP (Fig. 1*C*; see Notes) and single-neuron activity across limbic circuits in awake, nonrestrained conditions. Electrophysiological and behavioral recordings were conducted for 20 min (10 min while mice were awake in their home cage followed by 10 min while mice performed the elevated zero-maze task). First, we set out to determine whether NAC low-gamma oscillations modulated local single-unit activity by using data from the home cage recording segment (Fig. 1*D*). We found that 16% (three of 18) of NAC neurons were phase-locked to NAC low-gamma oscillations. No-

tably, when we limited our phase-locking analysis to recording segments consistent with high NAC low-gamma oscillatory amplitude (>2 SD of mean oscillatory amplitude), we found that 28% (five of 18) of our recorded NAC neurons phase-locked to low-gamma oscillations. Additionally, the degree of phase-locking was significantly increased in all five of the phase-locked NAC neurons during high NAC low-gamma amplitude LFP segments ($Z = 7.6 \pm 2.9$ during all NAC low-gamma amplitude LFP segments vs $Z = 20.7 \pm 5.0$ during high NAC low-gamma amplitude LFP segments; $p < 0.05$ using paired t test). Together, these results suggested that NAC low-gamma oscillations reflected locally relevant brain activity.

Next, we set out to determine whether this neural oscillatory mode contributed to interstructural mesolimbic circuit function. The NAC receives afferent input from multiple mesolimbic areas including glutamatergic projections from BA, PrL_Cx, and V. Hipp, and dopaminergic projections from VTA. Given that LFP oscillatory synchrony has been implicated in mediating long-range communication across brain areas during spatial cognitive processing and fear processing (Seidenbecher et al., 2003; Jones and Wilson, 2005; Dzirasa et al., 2009; Adhikari et al., 2010), we investigated whether any of the brain areas we recorded displayed oscillatory synchrony with NAC in the low-gamma frequency range. Consistent with previous reports (Popescu et al., 2009), we found that BA displayed low-gamma synchrony with NAC. Additionally, we observed low-gamma synchrony between NAC and VTA as well (Fig. 1*E*). When we compared NAC–BA and NAC–VTA synchrony across WT mice, we found that the degree of NAC–BA synchrony was negatively correlated with the tendency of mice to enter the open segment of the maze (as measured by the number of open segment entries normalized by the total distance traveled on the zero maze; $p = 0.02$, $r = 0.72$) (Fig. 1*F*). Additionally, the ratio of NAC–VTA/NAC–BA low-gamma synchrony observed across mice was positively correlated with the tendency of mice to explore the open segment of the maze (as measured by total time spent in the open segments normalized by the total distance traveled on the zero maze; $p = 0.005$, $r = 0.81$) (Fig. 1*G*). Notably, the NAC–VTA/NAC–BA ratio better predicted the tendency of mice to explore the open segment of the maze than NAC–VTA low-gamma synchrony ($p = 0.56$, $r = 0.21$) or NAC–BA synchrony alone ($p = 0.037$, $r = 0.66$). Importantly, NAC–BA and NAC–VTA synchrony values observed across mice did not simply reflect changes in behavioral profiles that occurred during exposure to the maze. Rather, NAC–BA and NAC–VTA synchrony values reflected the functional properties of the anxiety-related circuits since the LFP oscillation segments used for analysis were recorded while mice were immobile in their home cage (i.e., quiet waking) immediately before their first and only exposure to the zero-maze task.

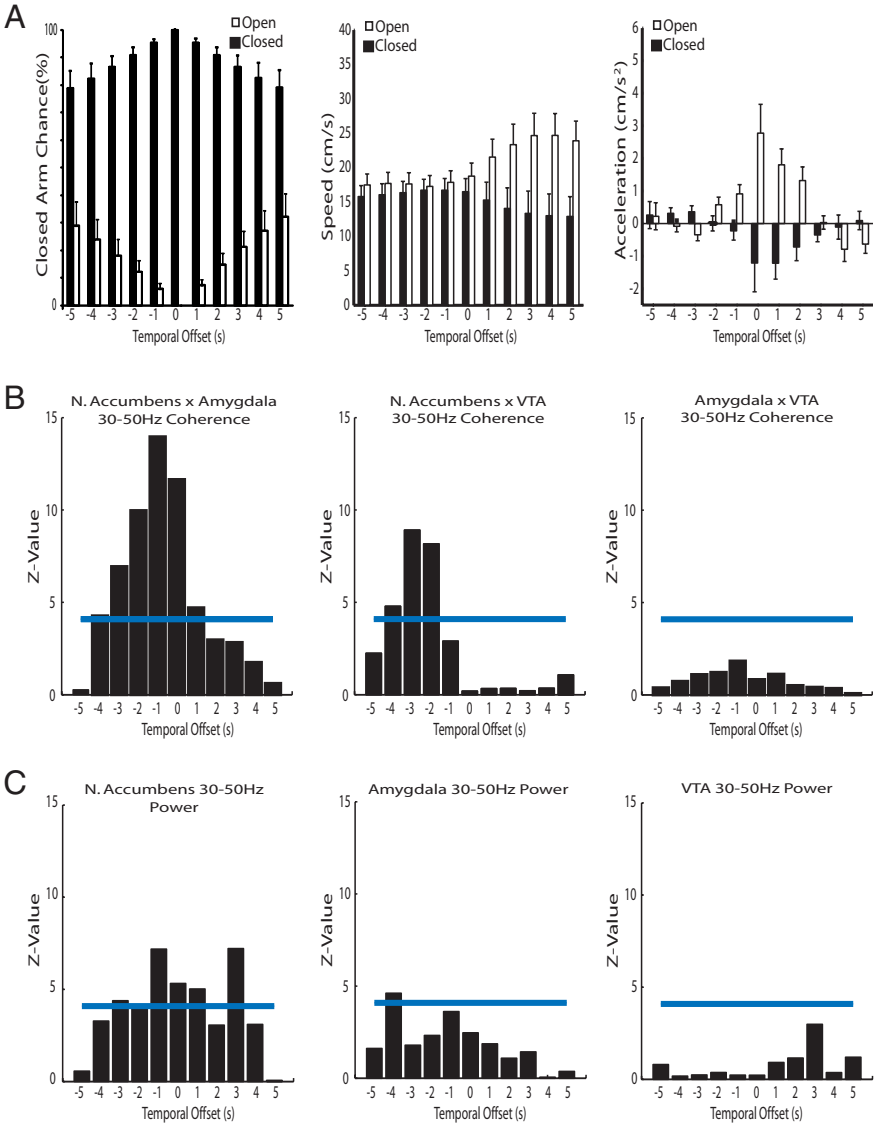

Figure 2. NAC interstructural synchrony varies during anxiety-related behaviors. ***A***, Open and closed segment interval location, speed, and acceleration profiles at various temporal offsets in WT mice. ***B***, p values for comparisons between open and closed segment cross-structural synchrony values measured at various temporal offsets ($Z = -\ln P$). ***C***, p values for comparisons between open and closed segment power values measured at various temporal offsets ($Z = -\ln P$). Statistical significance was determined for each frequency band using a GEE statistic followed by a Bonferroni correction. Blue lines depict the significance threshold. N., Nucleus.

After demonstrating that basal NAC–BA and NAC–VTA synchrony predicted anxiety-related behaviors, we set out to investigate whether the modulation of NAC–BA and NAC–VTA circuits mediated zero-maze task performance. First, we identified all of the 1 s intervals where mice were located in the open or closed segments of the zero maze and introduced temporal offsets ranging from −5 to 5 s into the recorded neurophysiological data. It is important to emphasize that the location of an animal in the zero maze (i.e., open vs closed segment) was not fixed for each temporal offset. For example, WT mice displayed a 29% chance of being in the closed segment 5 s before an open interval and a 79% chance of being in the closed segment 5 s before a closed segment interval (Fig. 2*A*). Next, we used generalized estimating equations to compare inter-area synchrony values measured during open intervals to those observed during closed

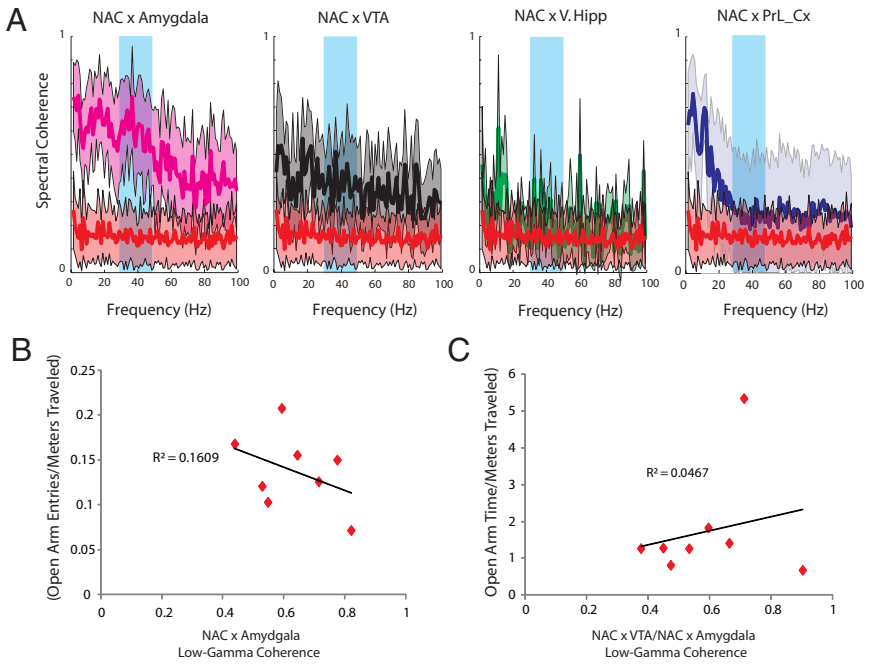

Figure 3. Anxiety-related circuit dysfunction in *Clock*-Δ19 mice. ***A***, Cross-spectral synchrony between NAC, BA, VTA, ventral hippocampus (V. Hipp), and PrL_Cx in *Clock*-Δ19 mice ($n = 543, 478, 82$, and 326 LFP pairs, respectively; figures depict mean ± SD, synchrony thresholds calculated using our bootstrapping method are shown in red). ***B***, ***C***, Home cage spectral coherence fails to correlate with anxiety-related behaviors in *Clock*-Δ19 mice. Regression lines are shown in black.

intervals at each of the temporal offsets. We found that NAC–BA synchrony was significantly increased during open intervals (compared with closed intervals) at zero temporal offset and offsets ranging from −4 to 1 s (but not more positive temporal offsets >1 s) (Fig. 2*B*; see Notes). Notably, since similar location profiles were observed at negative and positive temporal offsets (Fig. 2*A*, compare likely locations at +3 and −3 s temporal offsets), the significant NAC–BA synchrony differences observed between open and closed segment intervals at negative offsets did not simply reflect the fact that mice displayed a higher chance of being in the open segment before open intervals than before closed intervals. We found no significant differences in NAC–VTA gamma synchrony when we compared values measured during open intervals to values measured during closed intervals (i.e., zero temporal offset); however, NAC–VTA synchrony was significantly higher during open segment intervals at negative temporal offsets ranging from −4 to −2 s (compared with closed segment intervals at similar offsets) (Fig. 2*B*). Importantly, no significant open versus closed segment interval differences were observed in BA–VTA low-gamma synchrony at any temporal offsets, providing evidence that changes in NAC–BA and NAC–VTA low-gamma synchrony observed during zero-maze task performance were not due to gross volume conduction of LFP oscillatory signals or signal artifacts introduced at the ground screw references. Finally, we tested whether changes in NAC, BA, and VTA low-gamma oscillatory power reflected the location of mice on the zero maze (Fig. 2*C*). Although NAC low-gamma oscillatory power was increased in the open segments of the maze at temporal offsets ranging from −3 to 3 s, and BA low-gamma power was increased in the open segments at −4 s offset, these differences were much less pronounced than the changes observed in NAC–BA synchrony during performance of the zero-maze task. Additionally, no differences in open versus closed segment VTA oscillatory power were observed at any of the temporal offsets examined. Together, these findings support the hypothesis that dynamic changes in NAC–BA and NAC–VTA synchrony reflect neurophysiological circuit changes underlying the expression of anxiety-related behaviors.

After quantifying the dynamic changes in NAC–BA and NAC–VTA synchrony that occurred during the zero-maze task performance in WT mice, we set out to examine whether any of these neurophysiological processes were altered in *Clock*-Δ19 mice. Consistent with previous reports seen in *Clock*-Δ19 mice using an elevated plus-maze task (Roybal et al., 2007), we found that *Clock*-Δ19 mice displayed a significantly increased number of entries into the open segment of the zero maze compared with WT mice (open arm entries: 7.8 ± 2.5 and 15.8 ± 2.7 in WT and *Clock*-Δ19 mice, respectively; $p < 0.05$ using Wilcoxon rank sum test; $n = 10$ and 8 for WT and *Clock*-Δ19 mice, respectively). Importantly, these group differences were still observed even after we normalized the number of open segment entries displayed by *Clock*-Δ19 mice by the total distance mice traveled during zero-maze task performance (normalized open arm entries: 0.09 ± 0.02 and 0.14 ± 0.03 cm in WT and *Clock*-Δ19 mice, respectively; $p < 0.05$ using Wilcoxon rank sum test). This suggested that the increased number of open segment entries displayed by the *Clock*-Δ19 mice were not simply due to hyperactivity in the mutants. We also found that *Clock*-Δ19 mice tended to spend a greater percentage of time in the open segment of the maze compared with WT mice; however, these differences did not reach statistical significance in this study (open segment time: 21 ± 6% in WT mice vs 29 ± 7.0% in *Clock*-Δ19 mice, $p > 0.05$). Nevertheless, given that previous studies with the *Clock*-Δ19 mice have shown that these mutants exhibit anxiety-related behavioral deficits using four separate behavioral measures (Roybal et al., 2007), we are confident that the increased number of open segment entries observed using the zero-maze task corresponds with a true deficit in anxiety-related responses in *Clock*-Δ19.

Next, we analyzed neurophysiological data recorded while *Clock*-Δ19 mice were immobile in their home cage. We found that 42% (10 of 24) of the NAC neurons we recorded were phase-locked to low-gamma oscillations (during periods of high low-gamma amplitude, >2 SD), demonstrating that these NAC low-gamma oscillations reflected locally relevant brain activity in *Clock*-Δ19 mice as well. The percentage of phase-locked neurons in the *Clock*-Δ19 mice did not differ from the percentage of phase-locked neurons in WT mice ($p > 0.05$ using two-tailed Z test). We also found that both BA and VTA displayed low-gamma synchrony with NAC, consistent with findings observed in WT mice (Fig. 3*A*). However, NAC–BA synchrony in the home cage failed to correlate with the normalized number of open segment entries subsequently displayed across *Clock*-Δ19 mice ($p = 0.32$) (Fig. 3*B*), and the NAC–VTA/NAC–BA ratio failed to correlate with the normalized amount of time *Clock*-Δ19 mice spent in the open segment ($p = 0.61$) (Fig. 3*C*). *Clock*-Δ19 mice also failed to display significant changes in NAC–BA and NAC–VTA low-

gamma synchrony during zero-maze task performance at negative temporal offsets (Fig. 4*B*), despite the fact that these mice exhibited similar open and closed segment location profiles as WT mice at all temporal offsets ($p > 0.05$ for open and closed segment likelihood comparisons between WT and *Clock*-Δ19 mice at temporal offsets ranging from −5 to 5 s using Bonferroni corrected Student's *t* tests) (compare Fig. 4*A* with Fig. 2*A*). Moreover, *Clock*-Δ19 mice did not show open versus closed segment changes in NAC and BA low-gamma oscillatory power (Fig. 4*C*).

Finally, we wanted to determine whether the dysfunctional modulation of NAC–BA and NAC–VTA low-gamma synchrony observed during zero-maze task performance in *Clock*-Δ19 mice simply reflected changes in the behavioral profiles of these mice. *Clock*-Δ19 mice were hyperactive in the zero maze (distance traveled: 7920 ± 1183 cm in WT mice vs 11,024.5 ± 1127 cm in *Clock*-Δ19 mice, $p < 0.05$ using Wilcoxon rank sum test), and tended to move at higher speeds in the open segment (but not the closed segment) of the maze. However, no significant differences were observed between open and closed segment speeds at zero and negative temporal offsets (the temporal offsets at which the open vs closed segment changes in limbic synchrony were strongest in WT mice) for either genotype (see Notes), demonstrating that the limbic synchrony patterns observed at these offsets did not simply reflect changes in speed profiles based on the location of mice on the zero maze. Overall, these findings suggest that the altered synchrony patterns displayed by *Clock*-Δ19 mice at negative offsets do not simply reflect the higher open segment speeds exhibited by these mice.

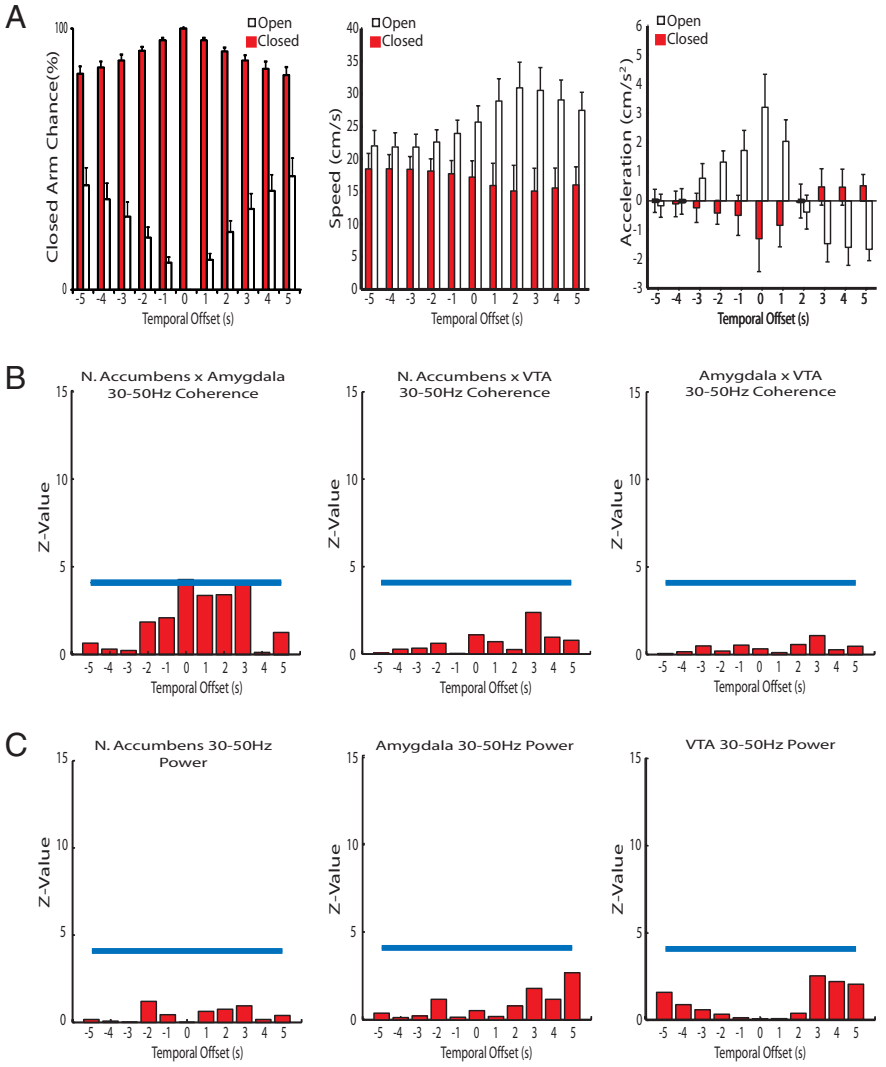

Figure 4. Anxiety-related circuit dysfunction during zero-maze task performance in *Clock*-Δ19 mice. ***A***, Open and closed segment interval location, speed, and acceleration profiles at various temporal offsets in *Clock*-Δ19 mice. ***B***, *p* values for comparisons between open and closed segment cross-structural synchrony values measured at various temporal offsets ($Z = -\ln P$). ***C***, *p* values for comparisons between open and closed segment power values measured at various temporal offsets ($Z = -\ln P$). Statistical significance was determined for each frequency band using a GEE statistic followed by a Bonferroni correction. Blue lines depict the significance threshold. Note that significant differences between open and closed segment synchrony and power values were not observed across the majority of the temporal offsets (compare with WT animal values depicted in Fig. 2). N., Nucleus.

Discussion

Cross-structural neural oscillatory synchrony has gained attention as a potential mechanism through which the brain binds the activity of populations of neurons distributed across many cortical and subcortical structures to generate percepts and behaviors. For example, studies have shown that the synchronization of rhinal and hippocampal oscillations reflects memory formation (Fell et al., 2001) and that hippocampus and prefrontal cortex oscillations synchronize during spatial–cognitive processes (Jones and Wilson, 2005; Dzirasa et al., 2009). Together, these studies suggest that the long-range synchronization of neural oscillatory activity may play a role in coordinating activity within and between structures that define broad neural circuits.

Here we use local field potentials recorded simultaneously across multiple limbic brain structures to identify a novel limbic circuit involved in mediating anxiety-related behaviors. Our findings demonstrate that basal NAC–BA low-gamma synchrony (observed while animals were immobile in their home cage) predicts the extent to which WT mice avoid the open segments of the zero–plus maze. Moreover, our findings show that NAC–BA low-gamma synchrony increases during periods when animals are in the open segments of the zero maze and during periods when animals display the highest tendency to transition into the open segments of the maze (i.e., zero and negative temporal offsets; see Notes). These findings suggest that NAC–BA synchrony likely reflects activity of circuits involved in fear-related processing. The ratio of NAC–VTA/NAC–BA low-gamma synchrony predicts the extent to which WT mice explore the open segment of the zero maze. We also show that NAC–VTA low-gamma synchrony increases during periods when animals display the highest tendency to transition into the open segment of the zero maze, but not during periods when animals were definitely in the open segments of the zero maze (zero temporal offset). Thus, these findings suggest that NAC–VTA low-gamma synchrony likely reflects the activity of circuits that coordinate exploratory behav-

iors. Notably, our findings do not exclude the possibility that synchrony between NAC and other limbic structures across different frequency bands (i.e., delta, theta, or high-gamma) may contribute to fear-related behaviors and anxiety related behaviors as well.

The NAC receives afferent projections from BA and VTA, two brain areas that have been shown to be critically involved in fear- and reward-related process. Since the behavioral output quantified using the zero-maze task ultimately reflects the influence of an anxiogenic stimulus (the elevated open segments of the maze) on exploratory behaviors, NAC low-gamma oscillations may reflect the activity of neurophysiological circuits that modulate the weight of fear- and reward-related circuits on decision making. Notably, our findings also demonstrate that a significant proportion of NAC neurons entrain to low-gamma oscillations (i.e., 28%). Although the overall number of NAC single neurons that we examined in this study was relatively small, a similar proportion of NAC low-gamma entrained neurons (i.e., 28%) was observed in a previous study (Popescu et al., 2009). Thus, our findings suggest NAC low-gamma oscillations are indeed locally relevant, and they support the hypothesis that nucleus accumbens low-gamma oscillations contribute to the synchronization of vast mesolimbic networks underlying the normal manifestation of anxiety-related behaviors in healthy mice.

Nearly all of the genes that control circadian rhythms are expressed in the limbic pathways, and studies have demonstrated that these genes play an important role in regulating behaviors associated with limbic circuit function (Abarca et al., 2002; McClung et al., 2005; Manev and Uz, 2006; Roybal et al., 2007; Lynch et al., 2008). For example, disruption of the circadian gene *Clock* leads to a striking behavioral profile including increased cocaine preference, decreased sleep, increased novelty-induced behavioral hyperactivity, and decreased depression-like behavior (Roybal et al., 2007). As such, *Clock*-Δ19 mice have been proposed as a model of human bipolar patients in the manic state. Bipolar disorder is a psychiatric illness that affects 1–3% of the US population and is characterized by manic and depressive symptoms (American Psychiatric Association, 2000). Anxiety is often comorbid with depression (Regier et al., 1993), and deficits in anxiety-related processing (i.e., increased risk-taking behavior) are associated with mania (Steiner, 1972). This suggests that the primary neurophysiological changes underlying bipolar disorder may lead to profound changes in anxiety-related circuit function. This hypothesis is supported by our neurophysiological findings in *Clock*-Δ19 mice. For example, we show that basal NAC–BA low-gamma synchrony fails to predict the extent to which *Clock*-Δ19 mice avoid the open segments of the zero-plus maze (as it had in WT mice), and the ratio of NAC–VTA/NAC–BA low-gamma synchrony fails to predict the extent to which *Clock*-Δ19 mice explore the open segment of the zero maze. Furthermore, *Clock*-Δ19 mice fail to display increases in NAC–BA and NAC–VTA low-gamma synchrony during periods in which animals displayed the highest tendency to transition into the open segments of the maze (i.e., zero and negative temporal offsets; see Notes). Since our previous findings demonstrate that the NAC low-gamma synchrony deficits observed in *Clock*-Δ19 mice directly correlate with their enhanced exploratory drive (Dzirasa et al., 2010), our findings suggest that the anxiety-related behavioral deficits observed in *Clock*-Δ19 mice may result from neurophysiological changes that directly or indirectly diminish the weight of fear circuits on decision making relative to the weight of reward circuits. Indeed, studies have demonstrated that *Clock*-Δ19 mice display increased bursting of dopaminergic neurons in VTA (McClung et al., 2005), and that VTA dopaminergic cell bursting is sufficient to drive reward-related behaviors (Tsai et al., 2009).

Overall, these findings demonstrate that NAC low-gamma oscillatory activity contributes to the synchronization of vast mesolimbic networks underlying the normal manifestation of anxiety-related behaviors in healthy mice. Moreover, our findings show that deficits in this neural oscillatory mode contribute to the circuit-level impairments that mediate anxiety-related behavioral dysfunction in *Clock*-Δ19 mice. Thus, our findings link the anxiety-related behavioral deficits observed in *Clock*-Δ19 mice with dysfunctional NAC low-gamma oscillatory tuning, and suggest that alterations in NAC oscillatory function induced by circadian gene polymorphisms may contribute to the anxiety-related behavioral manifestations seen in bipolar mania.

Notes

Supplemental material for this article is available at http://neurobiology.mc.duke.edu/faculty/nicolelis/Publications/JNeurosci_Impaired.pdf.

References

Abarca C, Albrecht U, Spanagel R (2002) Cocaine sensitization and reward are under the influence of circadian genes and rhythm. Proc Natl Acad Sci U S A 99:9026–9030.

Adhikari A, Topiwala MA, Gordon JA (2010) Synchronized activity between the ventral hippocampus and the medial prefrontal cortex during anxiety. Neuron 65:257–269.

American Psychiatric Association (2000) Diagnostic and statistical manual of mental disorders, DSM-IV-TR. Washington, DC: American Psychiatric Association.

Aouizerate B, Guehl D, Cuny E, Rougier A, Bioulac B, Tignol J, Burbaud P (2004) Pathophysiology of obsessive-compulsive disorder: a necessary link between phenomenology, neuropsychology, imagery and physiology. Prog Neurobiol 72:195–221.

Brog JS, Salyapongse A, Deutch AY, Zahm DS (1993) The patterns of afferent innervation of the core and shell in the "accumbens" part of the rat ventral striatum: immunohistochemical detection of retrogradely transported fluoro-gold. J Comp Neurol 338:255–278.

Crawley JN (1999) Behavioral phenotyping of transgenic and knockout mice: experimental design and evaluation of general health, sensory functions, motor abilities, and specific behavioral tests. Brain Res 835:18–26.

Dzirasa K, Ramsey AJ, Takahashi DY, Stapleton J, Potes JM, Williams JK, Gainetdinov RR, Sameshima K, Caron MG, Nicolelis MA (2009) Hyperdopaminergia and NMDA receptor hypofunction disrupt neural phase signaling. J Neurosci 29:8215–8224.

Dzirasa K, Coque L, Sidor MM, Kumar S, Dancy EA, Takahashi JS, McClung CA, Nicolelis MA (2010) Lithium ameliorates nucleus accumbens phase signaling dysfunction in a genetic mouse model of mania. J Neurosci 30:16314–16323.

Dzirasa K, Fuentes R, Kumar S, Potes JM, Nicolelis MA (2011) Chronic in vivo multi-circuit neurophysiological recordings in mice. J Neurosci Methods 195:36–46.

Fell J, Klaver P, Lehnertz K, Grunwald T, Schaller C, Elger CE, Fernández G (2001) Human memory formation is accompanied by rhinal-hippocampal coupling and decoupling. Nat Neurosci 4:1259–1264.

Gordon JA, Lacefield CO, Kentros CG, Hen R (2005) State-dependent alterations in hippocampal oscillations in serotonin 1A receptor-deficient mice. J Neurosci 25:6509–6519.

Greenberg BD, Gabriels LA, Malone DA Jr, Rezai AR, Friehs GM, Okun MS, Shapira NA, Foote KD, Cosyns PR, Kubu CS, Malloy PF, Salloway SP, Giftakis JE, Rise MT, Machado AG, Baker KB, Stypulkowski PH, Goodman WK, Rasmussen SA, Nuttin BJ (2010) Deep brain stimulation of the ventral internal capsule/ventral striatum for obsessive-compulsive disorder: worldwide experience. Mol Psychiatry 15:64–79.

Jacobs J, Kahana MJ, Ekstrom AD, Fried I (2007) Brain oscillations control timing of single-neuron activity in humans. J Neurosci 27:3839–3844.

Jones MW, Wilson MA (2005) Theta rhythms coordinate hippocampal-prefrontal interactions in a spatial memory task. PLoS Biol 3:e402.

Kalisch R, Korenfeld E, Stephan KE, Weiskopf N, Seymour B, Dolan RJ (2006) Context-dependent human extinction memory is mediated by a

ventromedial prefrontal and hippocampal network. J Neurosci 26: 9503–9511.
King DP, Zhao Y, Sangoram AM, Wilsbacher LD, Tanaka M, Antoch MP, Steeves TD, Vitaterna MH, Kornhauser JM, Lowrey PL, Turek FW, Takahashi JS (1997) Positional cloning of the mouse circadian clock gene. Cell 89:641–653.
LaBar KS, Gatenby JC, Gore JC, LeDoux JE, Phelps EA (1998) Human amygdala activation during conditioned fear acquisition and extinction: a mixed-trial fMRI study. Neuron 20:937–945.
Laird NM, Ware JH (1982) Random-effects models for longitudinal data. Biometrics 38:963–974.
Laviolette SR, Lipski WJ, Grace AA (2005) A subpopulation of neurons in the medial prefrontal cortex encodes emotional learning with burst and frequency codes through a dopamine D4 receptor-dependent basolateral amygdala input. J Neurosci 25:6066–6075.
Lynch WJ, Girgenti MJ, Breslin FJ, Newton SS, Taylor JR (2008) Gene profiling the response to repeated cocaine self-administration in dorsal striatum: a focus on circadian genes. Brain Res 1213:166–177.
Manev H, Uz T (2006) Clock genes: influencing and being influenced by psychoactive drugs. Trends Pharmacol Sci 27:186–189.
McClung CA, Sidiropoulou K, Vitaterna M, Takahashi JS, White FJ, Cooper DC, Nestler EJ (2005) Regulation of dopaminergic transmission and cocaine reward by the Clock gene. Proc Natl Acad Sci U S A 102:9377–9381.
Nelson MJ, Pouget P, Nilsen EA, Patten CD, Schall JD (2008) Review of signal distortion through metal microelectrode recording circuits and filters. J Neurosci Methods 169:141–157.
Popescu AT, Popa D, Paré D (2009) Coherent gamma oscillations couple the amygdala and striatum during learning. Nat Neurosci 12:801–807.
Regier DA, Narrow WE, Rae DS, Manderscheid RW, Locke BZ, Goodwin FK (1993) The de facto US mental and addictive disorders service system: epidemiologic catchment area prospective 1-year prevalence rates of disorders and services. Arch Gen Psychiatry 50:85–94.
Roybal K, Theobold D, Graham A, DiNieri JA, Russo SJ, Krishnan V, Chakravarty S, Peevey J, Oehrlein N, Birnbaum S, Vitaterna MH, Orsulak P, Takahashi JS, Nestler EJ, Carlezon WA Jr, McClung CA (2007) Mania-like behavior induced by disruption of CLOCK. Proc Natl Acad Sci U S A 104:6406–6411.
Seidenbecher T, Laxmi TR, Stork O, Pape HC (2003) Amygdalar and hippocampal theta rhythm synchronization during fear memory retrieval. Science 301:846–850.
Shin LM, Liberzon I (2010) The neurocircuitry of fear, stress, and anxiety disorders. Neuropsychopharmacology 35:169–191.
Siapas AG, Lubenov EV, Wilson MA (2005) Prefrontal phase locking to hippocampal theta oscillations. Neuron 46:141–151.
Steiner J (1972) A questionnaire study of risk-taking in psychiatric patients. Br J Med Psychol 45:365–374.
Swanson LW (1982) The projections of the ventral tegmental area and adjacent regions: a combined fluorescent retrograde tracer and immunofluorescence study in the rat. Brain Res Bull 9:321–353.
Tsai HC, Zhang F, Adamantidis A, Stuber GD, Bonci A, de Lecea L, Deisseroth K (2009) Phasic firing in dopaminergic neurons is sufficient for behavioral conditioning. Science 324:1080–1084.
Vitaterna MH, King DP, Chang AM, Kornhauser JM, Lowrey PL, McDonald JD, Dove WF, Pinto LH, Turek FW, Takahashi JS (1994) Mutagenesis and mapping of a mouse gene, Clock, essential for circadian behavior. Science 264:719–725.
Zeger SL, Liang KY (1986) Longitudinal data analysis for discrete and continuous outcomes. Biometrics 42:121–130.